Polarization-resolved imaging of an ensemble of waveguide modes

D. N. Schimpf[1,2,*] and S. Ramachandran[1,3]

[1]*Photonics Center, Department of Electrical and Computer Engineering, Boston University, 8 Saint Mary's Street, Boston, Massachusetts 02215, USA*

[2]*Currently with: Center for Free-Electron Laser Science, DESY, Notkestrasse 85, Hamburg, D-22607, Germany*

[3]*e-mail: sidr@bu.edu*

Corresponding author: dschimpf@mit.edu

We demonstrate polarization-sensitive measurement of the modal content of waveguides by generalizing the classic rotating wave-plate-based polarimeter to wide-field optical low-coherence interferometry. The spatial phases of the modes are retrieved with principal component analysis. By applying this polarization-sensitive cross-correlation (C^2) imaging technique to the characterization of a few-mode fiber, we reveal that different modes experience distinct bend-induced birefringence in optical fibers. This polarization-resolved C^2 imaging is well suited for analyzing the impact of polarization on wave propagation in high-power fiber lasers as well as in mode-division-multiplexed communications systems.   © 2012 Optical Society of America

OCIS codes: 060.2310, 060.2270, 060.2320, 060.2330.

Novel designs of optical waveguides propel applications such as the development of high-power fiber-laser systems and mode-division-multiplexed (MDM) communications systems [1,2]. The modal content of the fibers impacts their performance, and it needs to be analyzed in a reliable way. Lately, mode-measurement methods have been demonstrated that make no assumptions about the optical waveguide under test. These techniques, namely, spatially and spectrally resolved (S^2) imaging and cross-correlated C^2 imaging, utilize the principle that different modes experience different group delays [3,4].

C^2 imaging uses an external reference beam that samples all the modes of the fiber under test [4,5,6]. A distinct advantage of this optical low-coherence interferometric method over self-interferometric techniques (e.g., S^2 imaging) is the capability to measure arbitrary modal content distributions. While both mode-imaging methods have revealed the intensity and phase, the measurement of polarization states of modes has not been demonstrated thus far. This is relevant for both the amplification dynamics of high-power fiber-lasers and signal propagation in MDM systems [2,7]. Polarization-resolved mode measurement on short time scales has been shown with a holographic apparatus [8]. However, this technique relies on prior knowledge about the optical properties of the waveguide, which may need to be measured beforehand.

In this Letter, we resolve the different states of polarization (SOP) of modes in an arbitrarily constructed beam of light. This implementation of C^2 imaging enables mode measurement with completeness hitherto not demonstrated with any other technique, to the best of our knowledge.

In a conventional polarimeter, as shown in Fig. 1(a), the SOP of one beam is analyzed (in terms of Stokes parameters) by rotating a quarter-wave plate (QWP) and detecting the intensity after transmission through a polarizer in a fixed position [9]. However, this approach cannot be employed for a superposition of modes since only one beam is detected, and thus, it cannot discriminate the different modes, each having their own SOP.

Figure 1(b) illustrates the combination of the polarimeter principle with an interferometer. The different modes that are contained in the probe beam are gated by optical low-coherence interferometry, and the SOP of each mode is analyzed by interference with a linearly polarized reference beam. As the interference projects the polarization of the probe beam onto a linear polarization, it essentially mimics the role of the polarizer in the conventional polarimeter. In the probe arm of the Mach–Zehnder interferometer, a QWP is placed behind the fiber under test, and for every QWP position, the mode intensities are retrieved from the interference term of the cross-correlation signal. It is worth noting that the beam
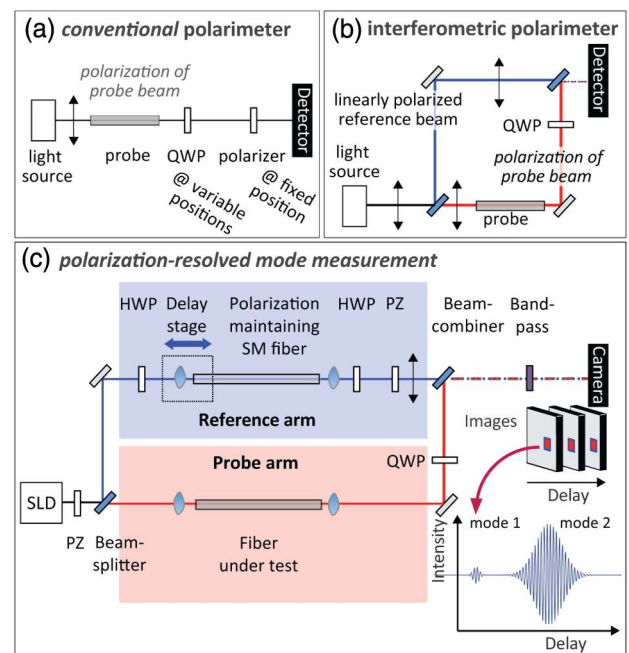

Fig. 1. (Color online) (a) Conventional polarimeter for the analysis of one beam, (b) interferometric analog that enables gating of the modes by coherence, (c) schematic of the experimental setup (PZ, polarizer; HWP, half-wave plate).

combiner must exhibit equal transmittance/reflectance for all SOP of light.

Figure 1(c) shows a schematic of the experimental setup. The light source is a superluminescent diode (SLD) (wavelength of 1054 nm). The fiber under test is placed in the probe arm. In the reference arm, a computer-controlled translation stage scans across the temporal delays of the modes of the probe waveguide. At each stage position, an image of the interference between the near-field of the fiber output and the collimated expanded beam of the reference arm is taken with a camera. In this way, at every pixel, the cross-correlation trace between the reference field and the different modes can be detected. In the reference arm, a polarization maintaining (PM) single-mode fiber ($L_r \approx 90$ cm) matches the dispersion between the two arms and avoids beam-walking. A filter with a bandpass of 5 nm is placed before the camera to increase the coherence length.

The intensity at the output, $I(x, y)$, is the sum of a delay-independent background term $I_0(x, y)$ and the delay-dependent interference terms of the reference with the different modes, $\sum_m I_{mr}(x, y, \tau)$, which can be written as follows [4]:

$$I_{mr} = 2\alpha_m \sqrt{i_m(x, y)} \sqrt{i_r(x, y)} \, \mathbf{Re}(g_{mr}(x, y, \tau)), \quad (1)$$

where α_m is the (amplitude) modal weight of the mode, $i_m(x, y)$ and $i_r(x, y)$ denote the transverse (normalized) intensity patterns of the fields, and g_{mr} stands for their cross correlation, which is given by

$$g_{mr} = (\mathbf{j}_m^* \cdot \mathbf{j}_r)(x, y) c_{mr}(\tau - \tau_{mr}) \exp(i\psi) \exp(i\delta\phi(x, y)), \quad (2)$$

where $\mathbf{j}_m$ and $\mathbf{j}_r$ are the local unit vectors (Jones vector) of the mode and the linearly polarized reference, respectively. Altering the polarization of the fiber output with a retardation plate allows determination of the SOP. The phase $\delta\phi(x, y)$ is the spatial phase of the mode, and ψ is given by $(\beta_m(\omega_0)L - \beta_r(\omega_0)L_r - \tau\omega_0)$, where $\beta_m(\omega_0)$ and $\beta_r(\omega_0)$ stand for the mode-propagation constants (at the center angular frequency ω_0) of the probe and reference fiber with lengths L and L_r, respectively. The signal of the cross correlation is illustrated in the inset of Fig. 1(c). In the cross correlation, several peaks appear for different modes at τ_{mr}, which is the group-delay difference between each mode and the reference beam. The high-frequency oscillation of the cross-correlation arises from the term $(\tau \cdot \omega_0)$ in ψ. The envelope of the cross-correlation trace is expressed by the function $c_{mr}(\tau - \tau_{mr})$, which is slowly varying with the delay variable $\tau = d/c_0$ where d is the delay-stage position. This "coherence gate" function c_{mr}, which is well known from optical coherence tomography, is related to the spectrum and the dispersion mismatch between the arms of the interferometer. An expression can be found in [4].

The data acquisition works as follows: we sample the cross-correlation trace at coarse steps (typically, less than 100 points per millimeter). At each of these points, we move the delay stage by a fraction of the wavelength (we chose $\lambda/12$). This fine stepping allows us to subtract the background intensity (which is the mean of the local

high-frequency oscillation) and to obtain the envelope (which is the maximum point). Furthermore, we retrieve the spatial phase based on the principal component analysis (PCA) algorithm [10]. It is asynchronous and does not need any *a priori* assumptions about the step size or the background term.

The SOP is characterized in terms of the Stokes parameters. As shown in Fig. 1(c), for different rotations of the fast axis of the QWP by an angle (Θ) with respect to the orientation of the polarization of the reference beam (which is parallel to the optical table), we acquire the interferometric signal as a function of translation-stage position. Analysis of the signal for every QWP position yields intensity maps of the retrieved modes as a function of Θ, $M_m(x, y) = \alpha_m^2 i_m(x, y) |\mathbf{j}_m^*(\Theta) \cdot \mathbf{j}_r|^2$. For one mode, these intensity maps M will, at every pixel (r, s), show the following form over Θ [9]:

$$M_{r,s}(\Theta) = c_0 + c_2 \cdot \cos(2\Theta) + c_4 \cdot \cos(4\Theta) + s_2 \cdot \sin(2\Theta)$$
$$+ s_4 \cdot \sin(4\Theta). \quad (3)$$

The (local) Stokes parameters are related to the (local) coefficients c_0, c_2, c_4, s_2, and s_4, which can be obtained by discrete and finite Fourier-series analysis (with respect to Θ) [9]. By minimizing the number of Θ-angle positions to six, i.e., $0, 1/6\pi, \ldots 5/6\pi$, we shorten the time of the data acquisition.

To quantify the accuracy of the interferometric polarimeter, we compare it to the conventional polarimeter. For this we insert PM single-mode fibers in both arms. The conventional polarimeter is obtained by blocking the reference arm and inserting a polarizer before the camera. For both types of polarization measurements, we produce polarized light along the horizontal direction and the 45° direction with wave-retardation plates after the fiber in the reference arm. In theory, these configurations correspond, respectively, to polarization states with Stokes parameters $(S_1, S_2, S_3)/S_0 = (1, 0, 0)$ and $(0, 1, 0)$. With the conventional polarimeter, the following experimental values (weighted by intensity, i.e., S_0) are obtained: (0.85, 0.10, 0.04) and (0.11, 0.99, 0.02). In independent interferometric measurements, we obtain (0.998, 0.04, 0.03) and (0.15, 0.97, 0.05). In this proof-of-principle configuration of our interferometric technique, the error in Stokes-parameter estimation is less than 15% and 5%, respectively, compared to the conventional polarimeter.

To demonstrate simultaneous SOP measurement in multiple modes, we use an anomalous dispersion higher order mode (HOM) fiber ($L \approx 90$ cm) [11]. Generally, C^2 imaging allows different fibers to be analyzed. We have previously characterized LMA fibers containing other modes such as LP_{11} and LP_{21}, which are known to deleteriously affect the performance of high-power fiber lasers [4]. In the present HOM fiber, a long-period grating partitions 46% energy into the LP_{01} mode and 54% into the LP_{02} mode of this fiber, over a 4 nm band centered at 1050 nm—our measurement wavelength range. Figure 2 displays the retrieved modes as a function of the rotation angle Θ of the QWP. It can be seen that the two modes show maximum amplitude values at different Θ angles. This results in a different Stokes parameter for the two
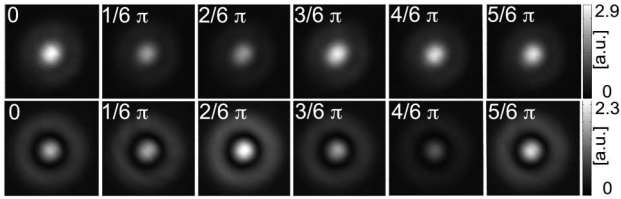
Fig. 2.   Retrieved mode-amplitude for LP_{01} (top) and LP_{02} (bottom) as a function of QWP angle Θ.
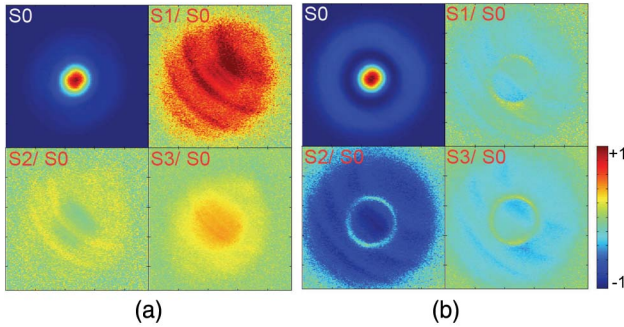

Fig. 3.   (Color online) (a), (b) Stokes-parameter maps for the LP_{01} and LP_{02} modes, respectively.
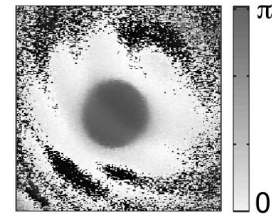

Fig. 4.   Retrieved phase of the LP_{02} mode.

In conclusion, we have demonstrated cross-correlated imaging of the modal content with the capability of resolving the polarization, as well as the spatial phase, for every mode in a superposition of modes. The accuracy of our method is within 15% of conventional SOP measurement techniques, but with the advantage of measuring multiple modes simultaneously. We employ our polarization-resolved mode imaging to the analysis of a non-polarization-maintaining few-mode fiber, and reveal that the SOP varies differently for distinct modes as postulated by waveguide theory. This makes the method valuable for studying the evolution of polarization in multimoded and few-moded fiber and waveguide systems.

modes. Figure 3 shows the retrieved Stokes parameter for the LP_{01} and LP_{02} modes. The LP_{01} mode shows a Stokes parameter S_1/S_0 close to 1, corresponding to a dominant polarization orientation along the x or y direction. The LP_{02}-mode shows a Stokes parameter S_2/S_0 close to -1, indicating a linear polarization direction along 45° or $-45°$. It is evident that the output SOP of LP_{01} and LP_{02} are not the same in spite of similar polarization at the input. This is expected of fibers, since different modes experience different birefringence, e.g., due to bending.

The phases of the individual modes are retrieved by the PCA algorithm. While the output of the test fiber is imaged on the camera, the collimated reference beam will generally show a residual phase. Thus, a retrieval of the phase of the fundamental mode (which should be flat) enables us to measure this phase. We subtract it from the retrieved phase of the HOMs, yielding the phase patterns for the HOMs. The phase of the LP_{02} mode exhibits the expected π-phase step, as shown in Fig. 4. This π-phase shift corresponds to a flip of the polarization, which cannot be resolved from a Stokes-parameter measurement.

References

1. D. J. Richardson, J. Nilsson, and W. A. Clarkson, J. Opt. Soc. Am. B **27**, B63–B92 (2010).
2. R. Ryf, S. Randel, A. H. Gnauck, C. Bolle, A. Sierra, S. Mumtaz, M. Esmaeelpour, E. C. Burrows, R.-J. Essiambre, P. J. Winzer, D. W. Peckham, A. H. McCurdy, and R. Lingle, J. Lightwave Technol. **30**, 521 (2012).
3. J. W. Nicholson, A. D. Yablon, S. Ramachandran, and S. Ghalmi, Opt. Express **16**, 7233 (2008).
4. D. N. Schimpf, R. A. Barankov, and S. Ramachandran, Opt. Express **19**, 13008 (2011).
5. Y. Z. Ma, Y. Sych, G. Onishchukov, S. Ramachandran, U. Peschel, B. Schmauss, and G. Leuchs, Appl. Phys. B **96**, 345 (2009).
6. P. Nandi, Z. Chen, A. Witkowska, W. J. Wadsworth, T. A. Birks, and J. C. Knight, Opt. Lett. **34**, 1123 (2009).
7. A. V. Smith and J. J. Smith, Opt. Express **19**, 10180 (2011).
8. D. Flamm, O. A. Schmidt, C. Schulze, J. Borchardt, T. Kaiser, S. Schröter, and M. Duparré, Opt. Lett. **35**, 3429 (2010).
9. H. G. Berry, G. Gabrielse, and A. E. Livingston, Appl. Opt. **16**, 3200 (1977).
10. J. Vargas, J. Antonio Quiroga, and T. Belenguer, Opt. Lett. **36**, 1326 (2011).
11. S. Ramachandran, S. Ghalmi, J. W. Nicholson, M. F. Yan, P. Wisk, E. Monberg, and F. V. Dimarcello, Opt. Lett. **31**, 2532 (2006).